

# EXPERIMENTAL INVESTIGATION OF SPHERICAL-FLAME ACCELERATION IN LEAN HYDROGEN-AIR MIXTURES

Bauwens, C.R.L.<sup>1,2</sup>, Bergthorson, J.M.<sup>2</sup> and Dorofeev, S.B.<sup>1</sup>

<sup>1</sup> FM Global, Research Division, 1151 Boston-Providence Turnpike, Norwood, 02062, USA

<sup>2</sup> McGill University, Department of Mechanical Engineering, Montreal, H3A 0G4, Canada

## ABSTRACT

Large-scale experiments examining spherical-flame acceleration in lean hydrogen-air mixtures were performed in a 64 m<sup>3</sup> constant-pressure enclosure. Equivalence ratios ranging from 0.33 to 0.57 were examined using detailed front tracking for flame diameters up to 1.2 m through the use of a Background Oriented Schlieren (BOS) technique. From these measurements, the critical radii of onset of instability for these mixtures, on the order of 2-3 cm, were obtained. In addition, the laminar burning velocity and rate of flame acceleration as a function of radius were also measured.

## 1.0 INTRODUCTION

As the prevalence of hydrogen throughout industry has increased, the potential for an accidental release of a large quantity of hydrogen has become a greater concern. Due to the high reactivity of the fuel, and its wide detonability range, mitigation mechanisms such as ventilation or limitations on the total storage quantity are commonly used to reduce the hazard in buildings and enclosures. Nevertheless, there may be situations where the formation of lean hydrogen-air mixtures that are above the lower flammability limit cannot be prevented. Lean hydrogen-air flames are particularly sensitive to the formation of hydrodynamic instabilities which accelerate the flames. Traditionally the laminar burning velocity alone is used as a baseline fuel reactivity parameter to model the behavior of the fuel, flame propagation and its interactions with turbulence and obstacles. If the development of flame instabilities are not taken into account, the flame propagation velocity and rate of heat release can be significantly under-predicted in such models. As a result, there is great interest in characterizing the behavior of lean hydrogen-air mixtures, in order to properly account for the development of flame instabilities.

The primary hydrodynamic instability that forms in all flames is generated by the Darrieus-Landau instability [1, 2], which been extensively observed throughout studies of spherical-flame propagation [3, 4, 5, 6]. Even in the absence of initial turbulence, spherical flames will spontaneously form cellular structures, resulting in flame acceleration due to an increase in flame surface area. For a given mixture, the radius at which these cells form is a material property, which is commonly normalized by flame thickness and expressed as a critical Peclet number [7, 8].

The increase in flame surface area, and the overall magnitude of acceleration, depends on the amplitude and wavelength of the structures that form. Previous studies have found that these flames accelerate indefinitely and their propagation velocities increase as a power law with time [9]. In atmospheric-pressure propane-air flames, it has been found that the flame velocity increases by a factor of 1.5 when the flame radius is between three to four times the critical radius [10]. This effect is of particular importance within the context of industrial safety, where the peak flame velocity is the primary factor that determines the pressures that develop. This effect is considerably more severe in lean hydrogen-air mixtures, which have significantly smaller critical radii such that a greater acceleration can be obtained at the same physical radius.

In the work of Gostintsev et al. [9, 11], it was suggested that the sustained acceleration is a result of ongoing cell splitting which generates fractal structures of the flame surface. In a previous study examining propane-air mixtures [10], oscillatory flame acceleration was observed with frequency intervals consistent with the concept of cell splitting and the formation of fractal structures. Based on these results, the original power law relation of Gostintsev et al. [9] was reformulated and the following relationship between propagation velocity and flame radius was obtained [10]:

$$u/u_L = (R/R_0)^\beta. \quad (1)$$

where  $u_L$  is the laminar flame propagation velocity of the mixture,  $R_0$  is the critical radius of onset of instability, and  $\beta$  is a fractal excess that can be obtained experimentally. This result suggests that the critical radius is an integral parameter in characterizing the overall mixture reactivity in general and, specifically, in determining the overall propagation velocity of a spherical flame at a given radius.

The objective of this study is to characterize the rate of spherical-flame acceleration for lean atmospheric-pressure hydrogen-air flames in a large-scale enclosure. This includes performing detailed front tracking to capture the flame radius as a function of time for flames up to 1.2 m in diameter, and determine the critical radius and fractal excess needed for Eq. (1). In addition, other phenomena seen in past studies, such as oscillatory flame acceleration [10] and the possibility of multiple regimes of flame acceleration [6] will also be examined.

## 2.0 EXPERIMENTAL SETUP

The overall experimental setup used in this study follows closely that of a previous study [10], where a full description of the test setup and instrumentation can be found. The experiments were performed in a 64 m<sup>3</sup> vented enclosure with dimensions of 4.6 × 4.6 × 3.0 m<sup>3</sup>, as shown in Fig. 1, with a single 5.4 m<sup>2</sup> vent to maintain a constant internal pressure during flame propagation. Ignition was supplied by an automotive ignition system using two 50 μm tungsten wires as electrodes and the overall ignition energy was estimated to be less than 100 mJ. A thin polypropylene sheet was used to contain the initial mixtures during filling and mixing. The sheet was cut prior to each test and held in place using pneumatic clamps that were released 1 s prior to ignition.

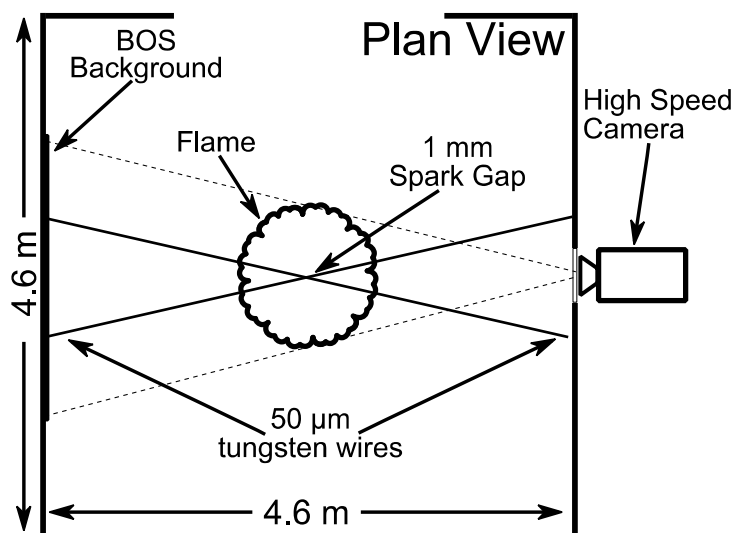


Figure 1. Schematic of the enclosure and ignition configuration.

A range of hydrogen-air concentrations were examined with equivalence ratios,  $\phi$ , ranging from  $\phi = 0.33 - 0.57$  (12.3 – 19.2% hydrogen in air by volume). This range of concentrations was selected to limit the effect of buoyancy, for the lean limit, and ensuring that the maximum pressures that develop within the enclosure were below the design strength of the enclosure, for the upper concentration limit. The initial mixtures were prepared by injecting research grade hydrogen from a port at the center of the floor of the enclosure. Four large diameter mixing fans in a counter-flow arrangement were used to produce a uniform composition throughout the enclosure. The fans were stopped five minutes prior to ignition to ensure a quiescent initial mixture, with turbulent fluctuations  $u' \ll 0.05$  m/s. The initial concentration was continuously monitored prior to ignition using an Illinois Systems P710 paramagnetic oxygen analyzer. Overall experimental uncertainty in mixture equivalence ratio was estimated to be within  $\phi \pm 0.015$ .

As the hydrogen-air flames did not emit sufficient radiation in the visible range to allow for direct tracking of the propagation of the flame, a Background Oriented Schlieren (BOS) technique was used. The background images were captured using a Vision Research Phantom Flex high speed camera for flame diameters up to 1.2 m. The flame propagation velocity was calculated from flame radii extracted from  $1,600 \times 1,600$  pixel images captured at a rate of 2,000 frames per second and the onset of cellular instability was extracted from the image sequence using the procedure described in the previous study [10]. Due to the smaller critical radii produced in lean hydrogen-air flames, however, the smoothing algorithm was reduced to a second order Savitzky-Golay filter with a window size of 5 ms to better capture the initial flame propagation.

### 3.0 BACKGROUND ORIENTED SCHLIEREN TECHNIQUE

The Background Oriented Schlieren (BOS) technique [12] allows for the generation of schlieren images without the need for any specialized optics by tracking the displacement of a background pattern due to the density gradients present in the imaged volume. This allows for schlieren measurements to be performed at large scale economically, however, the spatial resolution is sacrificed as the features in the background pattern must be larger than a single pixel and the displacements are averaged over windows containing multiple pixels. The BOS method produces images analogous to schlieren images, varying with the first derivative of density. This method is well suited for capturing large-scale low-speed hydrogen-air flames when compared with other low cost techniques such as shadowgraphy [13], which varies with the second derivative of density and tends to be better suited for resolving sharp density gradients such as shock fronts.

The displacement of the background pattern is calculated in a similar manner as PIV measurements, where an optimal feature size has been found to be on the order of 2-3 pixels to accurately resolve the displacement [14]. For this study, a random color background dot pattern was generated with a minimum feature size of 2 pixels per dot. The different color channels, however, were offset from one another by one pixel to generate a final image with an apparent resolution of 1 pixel per dot, while still maintaining a sufficient dot size in each color channel to perform the PIV analysis. To add flexibility in adjusting the size of the image frame, additional dots with a characteristic size of 6 pixels were blended into the image, as shown in Fig. 2, to allow for tests to be performed at different focal lengths with a single background. The background pattern was printed on standard printer paper and protected by 1/8 inch thick polycarbonate sheets. To illuminate the background pattern, an array of 10 banks of powerful LED lights were bounced off of the ceiling of the chamber to illuminate background pattern while minimizing the direct glare that was observable from the camera.



Figure 2. Dot pattern used for the BOS technique.

For each test, a background image was generated by averaging 50 frames of the high-speed video prior to ignition to minimize the contribution of sensor noise. For each frame after ignition, which will be referred to as target frames, a new image with the same resolution as the background image is created and at each pixel location an  $n \times n$  window of pixels from the target and background images were cross correlated to find the average displacement of the window centered at that location. Multiple windows sizes of  $n = 16, 8,$  and  $4$  were used. The larger windows sizes were used to pre-shift the subsequent target windows to ensure a maximum overlap between the final  $4 \times 4$  pixel windows. To improve the contrast of the final image, the pixel intensity at each location was then calculated from the square root of the magnitude of the total displacement, normalized by the magnitude of the maximum displacement in the overall image. This routine was performed over the three color channels and averaged into a final image.

The results of the BOS technique on a  $\phi = 0.35$  hydrogen-air flame at a radius of 42 cm is shown in Fig 3a. These images were processed to find the flame radius and center point of the flame for each image using the technique described in the previous study [10]. To reduce noise and resolve additional details on the flame surface, each image was resized to a common length scale such that the resized flame radius was constant across the full image sequence. A Kalman filter was then applied to these images to perform temporal smoothing across the image set without introducing motion blur from flame propagation. As the formation and motion of the individual cells on the flame surface was slow relative to the imaging rate of the camera, temporal smoothing significantly sharpened the appearance of the individual cells compared to the base image, as shown in Fig. 3b and the extracted flame contour is shown in green. This technique was used to prepare the images presented in the following section.

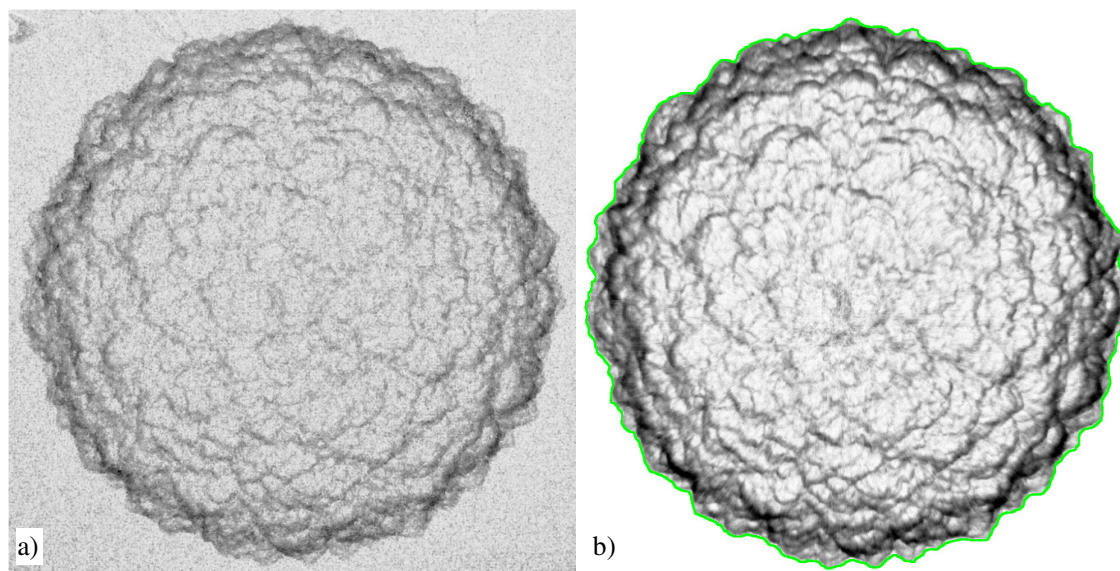


Figure 3. Background Oriented Schlieren images for a hydrogen-air flame with equivalence ratio of 0.35 at 42 cm radius. Raw BOS results (a) and results following temporal smoothing (b).

#### 4.0 RESULTS

A comparison of the structures seen on the flame surface over the full range of equivalence ratios for a number of flame radii is shown in Fig. 4. It can be clearly seen that there is little variation between the different equivalence ratios despite the overall flame propagation rate varying by factor of 3.5 between these concentrations. As the onset of cellular instability occurred when the flame radius was small, on the order of 40 – 80 pixels in diameter, the critical radius of instability could not be directly observed from the image sequence. Instead, the onset of cellular instability was captured from flame velocity which was in turn extracted from changes in flame cross-sectional area.









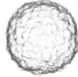
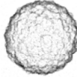
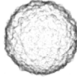
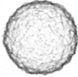
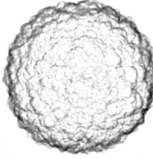
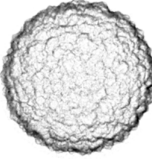
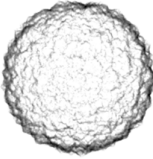
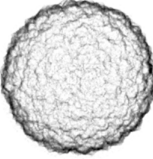
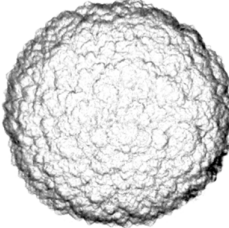
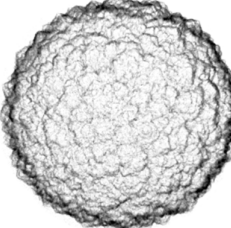
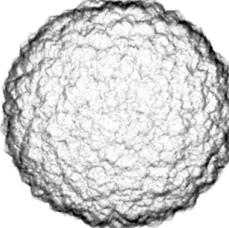
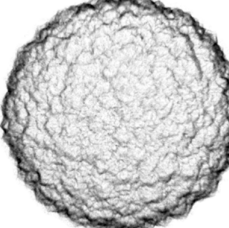
$\phi = 0.33$	$\phi = 0.40$	$\phi = 0.49$	$\phi = 0.57$
 16 ms	 12 ms	 6.5 ms	 4.5 ms
 31 ms	 22 ms	 12 ms	 9.0 ms
 55 ms	 40 ms	 22 ms	 16 ms
 98 ms	 70 ms	 38 ms	 28 ms
 170 ms	 121 ms	 64 ms	 48 ms

Figure 4. Flame surfaces of spherical hydrogen-air flames extracted from BOS for flame radii of 0.05, 0.10, 0.20, 0.40, and 0.60 m.

To determine the critical radius,  $R_0$ , and the unstretched laminar burning velocity,  $S_L$ , the observed flame propagation velocity,  $u_F$ , was plotted as a function of stretch rate, where stretch rate was defined as [15]:

$$\gamma = \frac{2}{R} u_F \quad (2)$$

as shown in Fig. 5. From these plots, the critical stretch rate at the onset of the cellular flame instability,  $\gamma_0$ , is clearly visible from which the corresponding radius,  $R_0$ , is extracted for each test. While recent studies suggest a non-linear extrapolation to zero stretch rate [16] to determine the laminar burning velocity, the results of this study are only used for comparison with past experimental data that used linear extrapolations, and, for consistency, a linear extrapolation was used.

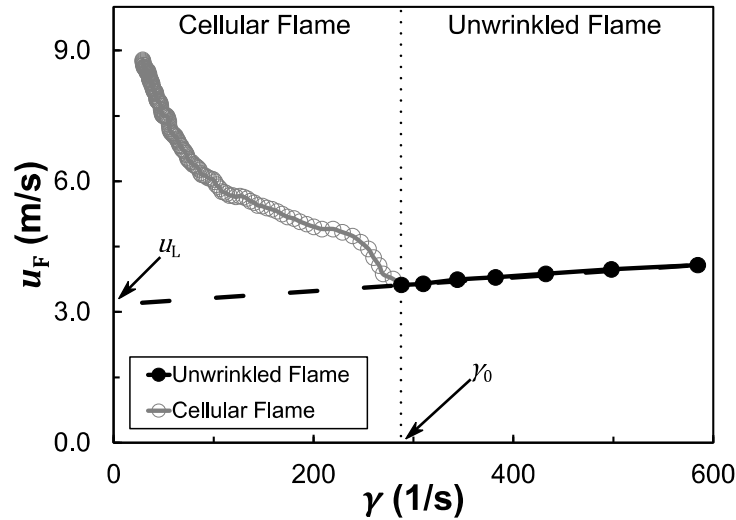


Figure 5. Determination of critical stretch rate and extrapolation to unstretched laminar flame propagation velocity for a  $\phi = 0.49$  hydrogen-air mixture.

Throughout the series of experiments performed, excellent agreement was found between the laminar burning velocities obtained in this study and past studies [17, 18, 19], as shown in Fig. 5, despite the experiments being performed at large scale using ambient conditions and with critical radii much smaller than maximum resolution of camera. These results were used to confirm that the correct rate of flame propagation was captured prior to the onset of flame instability and also gives a rough estimate for the overall measurement uncertainty of the experimental dataset.

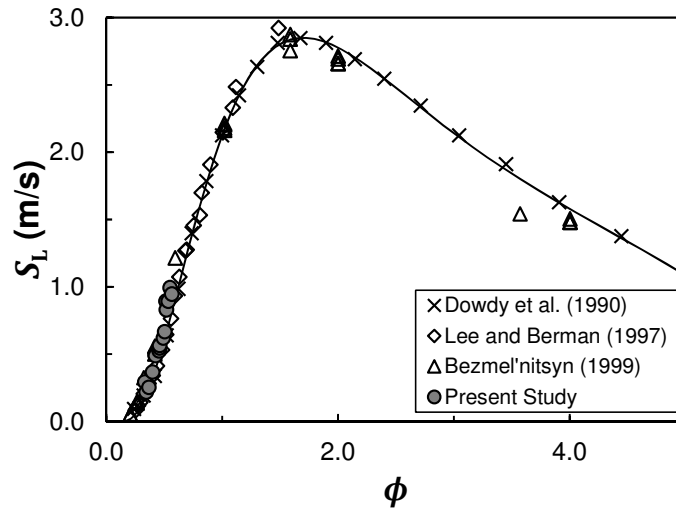


Figure 6. Unstretched laminar burning velocity of hydrogen-air mixtures at 298 K and 1 atm.

A summary of the initial test conditions and experimental results are provided in Table 1 where  $T$  is the initial temperature of the mixture,  $R.H.$  is the initial relative humidity,  $S_L$  is the extrapolated unstretched laminar burning velocity, and  $\mathcal{L}_M$  is the Markstein length of the mixture taken from the literature [20].

Table 1: Summary of test conditions and experimental results.

$\phi$	$T$ (K)	$R.H.$ (%)	$S_L$ (m/s)	$\gamma_0$ (s <sup>-1</sup> )	$R_0$ (mm)	$\mathcal{L}_M$ [20] (mm)
0.33	299	72	0.29	149	18	-0.61
0.35	300	38	0.22	137	18	-0.59
0.37	299	61	0.29	153	19	-0.55
0.40	300	58	0.37	223	19	-0.50
0.42	300	58	0.51	230	22	-0.46
0.42	299	45	0.49	231	22	-0.46
0.46	297	52	0.55	264	24	-0.40
0.46	297	85	0.55	280	23	-0.40
0.46	303	59	0.56	284	21	-0.40
0.49	300	42	0.63	288	25	-0.35
0.51	305	54	0.67	362	22	-0.32
0.52	301	42	0.89	362	26	-0.31
0.52	299	39	0.83	379	26	-0.30
0.54	307	50	0.89	399	25	-0.28
0.55	300	35	0.99	427	26	-0.26
0.57	298	46	0.95	387	30	-0.23

As the flame thickness estimate used in the previous studies [7, 8, 10] performs poorly for lean hydrogen-air mixture, the critical radius and Markstein length of these flames were compared directly instead of in terms of the dimensionless Markstein number and critical Peclet number. Figure 7 shows that the critical radius was found to decrease roughly linearly with Markstein length from 30 to 18 mm over the range of concentrations examined. The observed scatter was primarily due to the coarse temporal resolution in determining the critical stretch rate as the scatter was roughly equivalent to the change in radius that occurs over one frame of the image sequence as well as the uncertainty in the initial concentration.

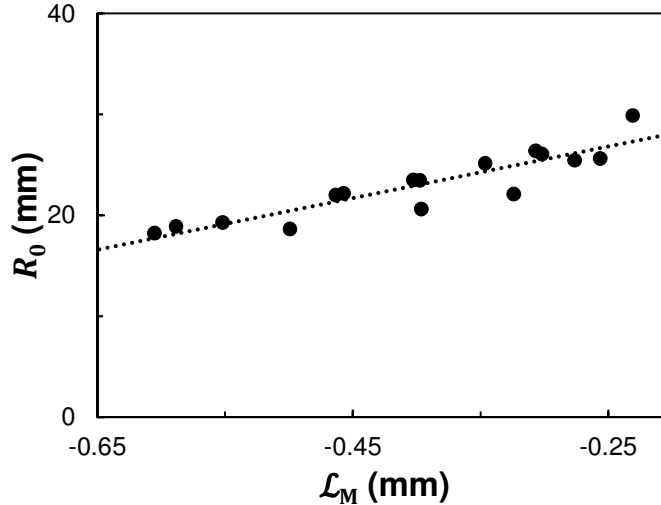


Figure 7. Critical radius for onset of Darrieus-Landau instability as a function of Markstein length.

## 5.0 DISCUSSION

Immediately following the onset of the cellular instability, the flame accelerates. To compare the rate of flame acceleration with the relationship described by Eq. (1), a normalized flame velocity,  $u_F/u_0$ , where  $u_0$  is the flame propagation velocity at the onset of cellular instability, must be compared with a

dimensionless flame radius,  $R/R_0$ . A power law fit of these variables produces a relation in the form  $u_F/u_0 = A(R/R_0)^\beta$ . The coefficient  $A$  was found to be approximately  $1.00 \pm 0.05$ . This scatter was likely caused by a combination of the variation in the initial acceleration of the first generation of cells that form on a smooth flame surface [10], as well as the uncertainty in resolving the critical radius. When the velocity was further normalized by  $A$ ,  $u^* = u_F/(A \cdot u_0)$ , which does not affect the exponent of power law relationship, all of the curves align with one another, as shown in Fig. 8, which is consistent with a constant fractal excess,  $\beta$ .

Throughout the full series of experiments, no oscillations in the rate of acceleration were observed. This is consistent with observations from a previous study for rich propane mixtures [10] for flames with negative Markstein length. It should also be noted that the fractal excess was not found to vary during flame acceleration, with the possible exception of initial cell formation, unlike a recent study where multiple regimes of spherical flame acceleration were suggested [6].

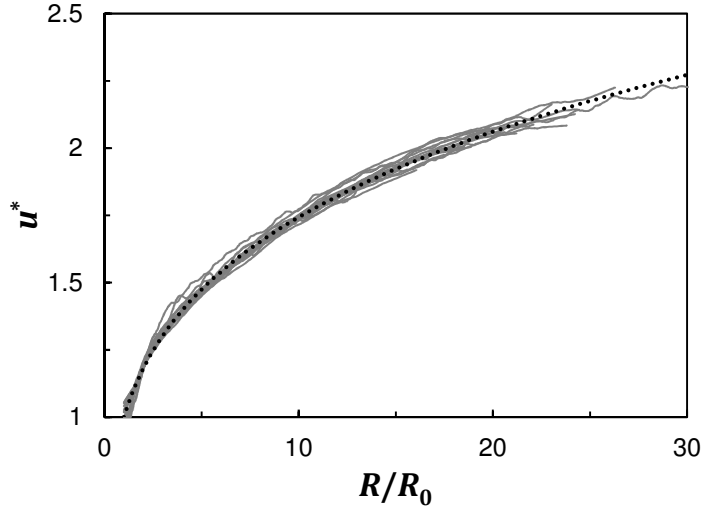


Figure 8. Normalized flame propagation velocity as a function of normalized flame radius compared to a simple power law with an exponent of 0.24.

The fractal excess,  $\beta$ , was found to be remarkably constant across all of the concentrations studied, as shown in Fig. 9, with an average value of  $\beta = 0.243 \pm 0.005$ . If this factor is converted in terms of time [10],  $R(t) = R_0(u_0 t/R_0)^{1/(1-\beta)}$ , the flame acceleration exponent for radius as a function of time,  $\alpha = 1/(1-\beta)$ , is found to be  $\alpha = 1.32 \pm 0.01$ , and is well within the range of 1.2 – 1.5 that has been found in prior studies [21].

To illustrate the effect of spherical flame acceleration in lean hydrogen-air flames, the results of Eq. (1) are extrapolated to larger flame radii in Fig. 10, while neglecting stretch effects. This plot shows that if the acceleration exponent remains constant to larger scales, as observed in other studies for a wide range of mixtures [9], the effective flame propagation velocity,  $u_{\text{eff}}$ , will continue to rise without any initial turbulence or obstacles, which would in turn further increase the flame propagation velocity. At a flame radius of one meter, a length scale consistent with an explosion in a small room, the burning velocity would increase to 2.4 – 2.6 times the laminar burning velocity. At a flame radius of ten meters, a length scale that could be reached during an explosion in a large enclosure or building, the effective burning velocity increases to 4.1 – 4.6 times the laminar burning velocity. As the maximum pressures that develop typically scale with the square of the burning velocity, properly accounting for flame self-acceleration due to instabilities is of critical importance when modeling large or intermediate scale hydrogen-air explosions.



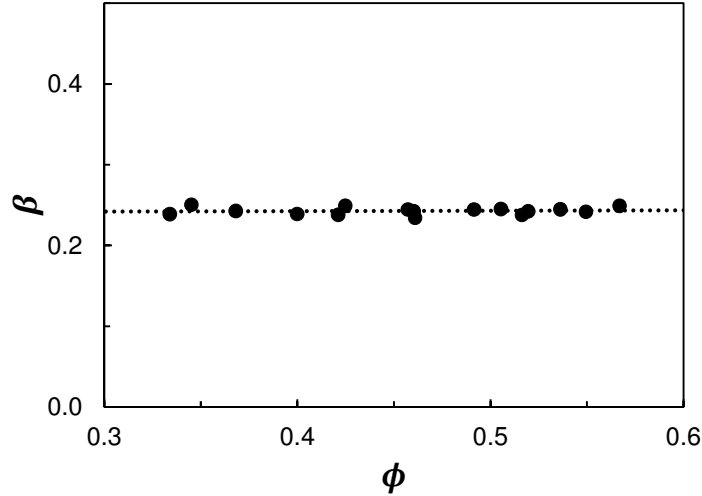


Figure 9. Fractal excess,  $\beta$ , as function of equivalence ratio.

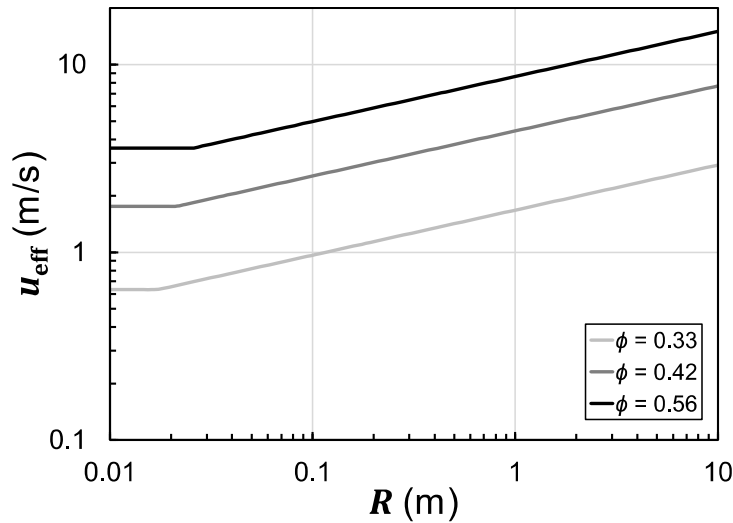


Figure 10. Extrapolated effective flame propagation velocity vs flame radius.

## 6.0 SUMMARY AND CONCLUSIONS

The critical radius for the onset of Darrius-Landau instability and the rate of flame acceleration for lean hydrogen-air mixtures was characterized using the Background Oriented Schlieren technique. Throughout the full series of experiments performed, the BOS technique produced high quality images, allowing for detailed measurements of the flame propagation velocity, the critical radius, and the laminar burning velocity of each mixture. Across the full range of equivalence ratios examined, significant acceleration was observed resulting in an increase in flame propagation velocity by a factor of two at a flame radius of 0.5 m.

Overall, the rate of spherical flame acceleration was consistent with the estimates from previous studies that attribute flame acceleration to the development of fractal structures on the flame surface. No oscillations in the rate of flame acceleration were observed in this study, consistent with past studies of mixtures with negative Markstein length. The flame acceleration exponent was not found to vary with concentration over the range of equivalence ratios examined. In addition, within each test, only a single regime of flame acceleration was observed which was not found to vary with time.

This study illustrates that significant flame acceleration is produced in lean hydrogen-air flames due to flame instabilities and that the effective reactivity of the fuel is highly dependent on the characteristic flame size. As a result, the effect of instabilities and their development with characteristic flame size on the burning velocity of these mixtures should be considered during the modeling of explosion hazards created by lean hydrogen-air mixtures at industrial scales.

## REFERENCES

1. G. Darrieus, unpublished work presented at La Technique Moderne, and at Le Congrès de Mécanique Appliquée, 1945 and 1938.
2. Landau, L.D., On the theory of slow combustion, *Acta Physicochim*, **19**, No. 1, 1944, pp. 77-85.
3. Istratov, A.G. and Librovich, V.B., On the stability of propagation of spherical flames, *Journal of Applied Mechanics and Technical Physics*, **7**, No. 1, 1966, pp. 43-50.
4. Bradley, D., Cresswell, T.M. and Puttock, J.S., Flame acceleration due to flame-induced instabilities in large-scale explosions, *Combustion and Flame*, **124**, No. 4, 2001, pp. 551-559.
5. Law, C.K., Jomaas, G., and Bechtold, J.K., Cellular instabilities of expanding hydrogen/propane spherical flames at elevated pressures: theory and experiment, *Proceedings of the Combustion Institute*, **30**, No. 1, 2005, pp. 159-167.
6. Kim, W.K., Mogi, T., Kuwana, K. and Dobashi, R., Self-similar propagation of expanding spherical flames in large scale gas explosions, *Proceedings of the Combustion Institute*, **35**, No. 2, 2015, pp. 2051-2058.
7. Bradley, D., Hicks, R.A., Lawes, M., Sheppard, C.G.W. and Woolley, R., The measurement of laminar burning velocities and Markstein numbers for iso-octane-air and iso-octane-n-heptane-air mixtures at elevated temperatures and pressures in an explosion bomb, *Combustion and Flame*, **115**, No. 1, 1998, pp. 126-144.
8. Gu, X.J., Haq, M.Z., Lawes, M. and Woolley, R., Laminar burning velocity and Markstein lengths of methane-air mixtures, *Combustion and Flame*, **121**, No. 1, 2000, pp. 41-58.
9. Gostintsev, Y.A., Istratov, A.G. and Shulenin, Y.V., Self-similar propagation of a free turbulent flame in mixed gas mixtures, *Combustion, Explosion, and Shock Waves*, **24**, No. 5, 1988, pp. 563-569.
10. Bauwens, C.R., Bergthorson, J.M. and Dorofeev, S.B., Experimental study of spherical-flame acceleration mechanisms in large-scale propane-air flames, *Proceedings of the Combustion Institute*, **35**, No. 2, 2015, pp. 2059-2066.
11. Gostintsev, Y.A., Fortov, V.E. and Shatskikh, Y.V., Self-similar propagation law and fractal structure of the surface of a free expanding turbulent spherical flame, *Doklady Physical Chemistry*, **397**, No. 1, 2004, pp. 141-144.
12. Settles, G.S., *Schlieren and shadowgraph techniques: Visualizing phenomena in transparent media*, 2001, Berlin:Springer-Verlag.
13. Dennis, K., Maley, L., Liang, Z. and Radulescu, M.I., Implementation of large scale shadowgraphy in hydrogen explosion phenomena, *International Journal of Hydrogen Energy*, **39**, No. 21, 2014, pp. 11346-11353.
14. Raffel, M., Willert, C.E., and Kompenhans, J., *Particle Image Velocimetry: a practical guide*, 1998, Berlin:Springer-Verlag.
15. Wu, C.K. and Law, C.K., On the determination of laminar flame speeds from stretched flames, *Proceedings of the Combustion Institute*, **20**, No. 1, 1985, pp. 1941-1949.

16. Wu, F., Liang, W., Chen, Z., Ju, Y. and Law, C.K., Uncertainty in stretch extrapolation of laminar flame speed from expanding spherical flames, *Proceedings of the Combustion Institute*, **35**, No. 1 2015, pp. 663-670.
17. Dowdy, D.R., Smith, D.B., Taylor, S.C. and Williams, A., The use of expanding spherical flames to determine burning velocities and stretch effects in hydrogen/air mixtures. *Proceedings of the Combustion Institute*, **23**, No. 1, 1991, pp. 325-332.
18. Lee, J.H. and Berman, M., Hydrogen combustion and its application to nuclear reactor safety, *Advances in heat transfer*, **29**, 1997, pp. 59-127.
19. Bezmel'nitzyn, A., Gavrikov, A., Kuznetsov, M., Denkevits, A. and Dorofeev, S.B., Experimental Study on Laminar Burning Velocities for Nuclear Safety Applications, Kurchatov Institute, Report No. 315/20116757/INR prepared for FZK-INR RRC, 1999.
20. Taylor, S.C., Burning velocity and the influence of flame stretch, 1991, Doctoral dissertation, University of Leeds.
21. Wu, F., Jomaas, G., & Law, C.K., An experimental investigation on self-acceleration of cellular spherical flames. *Proceedings of the Combustion Institute*, **34**, No. 1, 2013, pp. 937-945.